Anharmonic properties of raman modes in double wall carbon nanotubes

J. Marquina[a], CH. Power[b], J.M. Broto[c], E. Flahaut[d], and J. Gonzalez[b,e]

[a]*Centro de Estudios Avanzados en Óptica, Facultad de Ciencias,*
Universidad de los Andes, Mérida 5101, Venezuela.
e-mail: castella@ula.ve
[b] *Centro de Estudios en Semiconductores, Facultad de Ciencias,*
Universidad de los Andes, Mérida 5101, Venezuela.
[c] *Laboratoire National des Champs Magnétiques Intenses (LNCMI) - CNRS UPR*
3228, Université de Toulouse, 31400 Toulouse, France.
[d] *Laboratoire de Chimie des Matériaux Inorganiques (CIRIMAT), UMR CNRS*
5085, Université Paul Sabatier, 31062 Toulouse, France.
[e] *DCITIMAC-Malta Consolider Team, Universidad de Cantabria, Facultad de Ciencias,*
Santander 69005, Spain.

The temperature dependence of the radial breathing modes (RBMs) and the zone-center tangential optical phonons (G-bands) of double-walled carbon nanotubes (DWCNTs) has been investigated between 300 and 700 K using Raman scattering. As expected, with increasing temperature, the frequencies of the Raman peaks, including the RBMs and G-bands downshift simultaneously. We show here that the temperature dependence of the RBMs can be fitted by a simple linear dependence and different RBMs have different frequency shifts. We observe a noticeable nonlinearity in the temperature dependence of the G-band associated with the outer semiconducting tube G_{ext}^+ (s). The deviation from the linear trend is due to the contribution of the third-order anharmonic term in the lattice potential energy with a pure temperature effect. An estimated value of 1.5 for the Grüneisen parameter of the G_{ext}^+ (s) band was found.

Keywords: Raman spectroscopy; double wall carbon nanotubes; high-temperature; anharmonicity; Grüneisen parameter.

La variación con la temperatura de los modos de respiración radial (RBMs) y los fonones ópticos tangenciales de centro de zona (banda G) de los nanotubos de doble pared (DWCNTs) han sido investigados en el rango de 300 a 700 K utilizando dispersión Raman. Como era de esperarse, con el incremento de la temperatura las frecuencias de los picos Raman de los RBMs y las bandas G se desplazan hacia más bajas frecuencias. Nosotros demostramos que la variación con la temperatura de los RBMs puede ser ajustada mediante un modelo lineal y muestran diferentes desplazamientos en frecuencia. Nosotros observamos una no linealidad importante en la variación con la temperatura de la banda G asociada a los tubos semiconductores externos $\left(G_{ext}^+(s)\right)$. La desviación se debe a la contribución del termino anarmónico de tercer orden en la energía potencial. Se encontró un valor estimado de 1,5 para el parámetro de Grüneisen de la banda $G_{ext}^+(s)$.

Descriptores: Espectroscopia raman; nanotubos de carbono doble pared; altas temperaturas; anarmonicidad; parámetro Grüneisen.

PACS: 63.22.GH; 63.20.KG; 78.30.-J

1. Introduction

Carbon nanotubes have attracted intense scientific interest due to their fascinating essentially one-dimensional electronic and vibrational band structure, their unique mechanical properties as well as the prospect for numerous applications [1-3]. The double-wall carbon nanotube (DWCNT) is the most important member of the multi-walled carbon nanotube (MWCNT) family which can be produced in significant quantities [4]. These tubes consist of two concentric cylindrical graphene layers. Typical values of their inner and outer diameters range from approximately 0.40 to 2.5 nm and from approximately 1.0 to 3.2 nm, respectively [5-6]. These nano-objects made possible the study of low-dimensional crystal growth when the incorporated material is constrained to a few atomic layers in thickness by the encapsulating van der Waals surface of the carbon nanotubes. The preparation of highly anisotropic one-dimensional (1D) structures confined into CNTs in general is a key objective in carbon nanotube research [7-8].

The synthesis of mono-dimensional nanocrystals is complex due to the lack of stability of such structures. One way to stabilize them is to prepare them within a container, such as CNTs. CNTs are good candidates for this application due to their inner diameter being in the nanometer range, as well as their good chemical and thermal stability [4-6]. It has been shown recently that the DWCNTs can be filled with different materials: PbI_2 Fe, Te and others, opening a wide range of possible applications [7-8]. Also had been shows that DWCNTs quality can be improved by heat treatment [9].

Raman spectroscopy was shown to be a powerful and nondestructive technique for structural characterization of carbon nanotubes [10]. Raman spectroscopy at ambient pressure has been also successfully employed in the study of the more recently observed [8] and synthesized in bulk quantities [9] of double-wall carbon nanotubes (DWNTs), suggesting that the outer tubes provide an unperturbed environment to their interior [10] and that the interaction in a DWNT bundle is stronger than the inner-outer tube interaction [11].
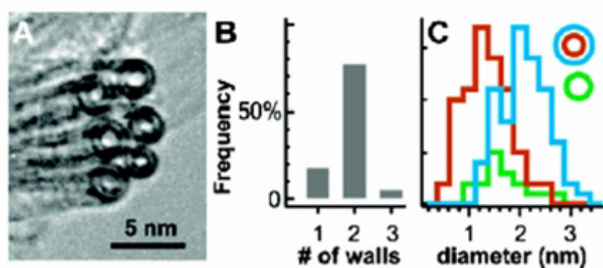
FIGURE 1. HRTEM images of DWCNTs A) High resolution bundle of DWCNTs B) Histograms of number of walls and C) internal and external diameter distribution for carbon nanotube samples plotted from 100 representative high resolution TEM images.

It is known that carbon nanotubes have strong temperature dependence [11-13], and all the phonons downshift with the increased temperature. In single-wall carbon nanotubes (SWCNTs) and DWCNTs has been found that the shifts in Raman frequencies for all peaks are linear as a function of the temperature [9, 12-13]. Nevertheless, more recently Zhou *et al.* [11] shows that the shift for G-band in DWCNTs and SWCNTs has a nonlinear relation with the increased temperature. They also have noted that the deviation from the linear trend is a consequence of the contribution of the third- and fourth-order anharmonic terms in the lattice potential energy with pure temperature effect.

In this letter, we present the results of a Raman spectroscopy study of the RBMs and G-bands at high temperatures in DWCNTs which were produced by a CCVD method. The temperature dependence of the Raman shift is analyzed in terms of thermal expansion and cubic anharmonic contribution. Four-phonon processes were not considered, since the temperature reached was not very high.

2. Experimental details

DWCNTs were synthesized by catalytic chemical vapor deposition (CCVD) as described in more detail in Ref. 6. A systematic analysis of TEM images (see Fig. 1) reveals that samples produced by this method contain approximately 77% of DWCNTs; the high proportion of DWCNTs was also confirmed by electron diffraction with a small admixture of about 18% of single-wall CNTs (SWCNTs), and roughly 5% triple-wall CNTs. The inner and outer diameters range from 0.53 to 2.53 nm and from 1.23 to 3.23 nm, respectively. The median inner diameter is 1.2 nm and the median outer diameter is 1.9 nm.

The Raman spectra of the DWCNTs were recorded at ambient pressure and temperature; in back-scattering geometry using a micro-Raman, triple grating system (DILOR XY800) equipped with a cryogenic CCD detector. The spectral resolution of the system was about 1 cm^{-1}. For excitation, the 514.5 nm line of an Ar$^+$ laser was focused on the sample by means of a 100X objective, while the laser power was kept below 2 mW, in order to avoid laser-heating effects on the probed material and the concomitant softening of the ob-

R1-Line Fluorescence Shift (cm^{-1})
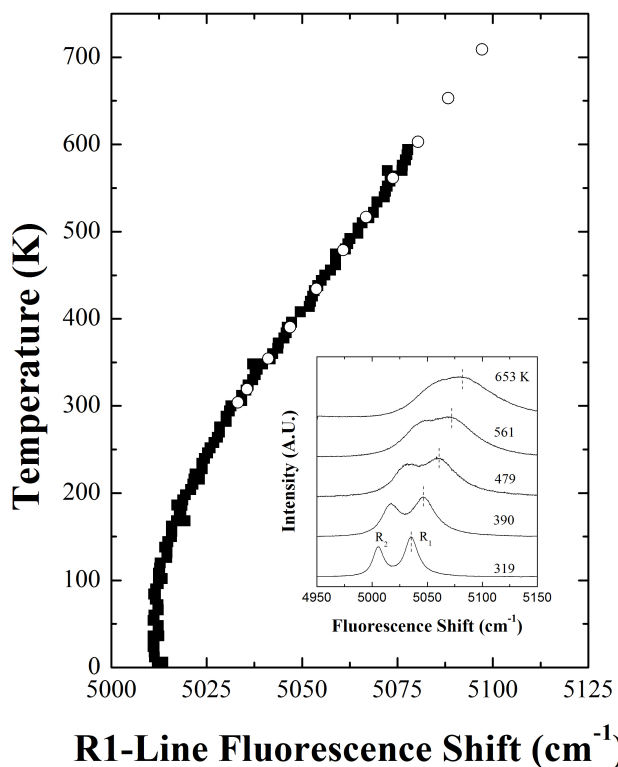
FIGURE 2. Variation of R1-line position vs temperature. Full squares: from [14]. Open circles: present values. The inset shows the intensity of ruby fluorescence as a function of Raman shift at various temperatures.

served Raman peaks. High-temperature measurements were carried out using a heating system "Watlow 96" in static air from 300 to 700 K. The temperature was obtained using small ruby spheres of around 5 μm diameter as the standard. Ruby is a chromium-doped form of corundum Al$_2$O$_3$ with Cr^{3+} substituted for aluminum ions. Ruby crystallizes in a close-packed hexagonal structure slightly distorted by repulsion between neighboring cations. Although the symmetry is reduced from cubic O_h to trigonal C_3 Ligand-field approach is quite reliable to describe electronic properties of ruby with low Cr^{3+} concentration. Assuming in first approximation a cubic field on the three d electrons of the Cr^{3+} ions, one can easily obtain electronic level diagrams by treating both trigonal distortion and spin-orbit interaction as perturbations. The first excited cubic state $2E$ is split by the interplay of both perturbations resulting in two Kramers' doublet ^2E and $^4A_2$. These two degenerate states are, respectively, responsible for intense and narrow emission lines R_1 and R_2 which occur around 14409 cm^{-1} at ambient conditions. The R_1 and R_2 lines are routinely used as *in situ* temperature sensors [14]. The R1-line position vs temperature given in Ref. 14 together with the present data is shown in Fig. 2. The inset shows the ruby fluorescence as a function Ramam shift for various temperatures.
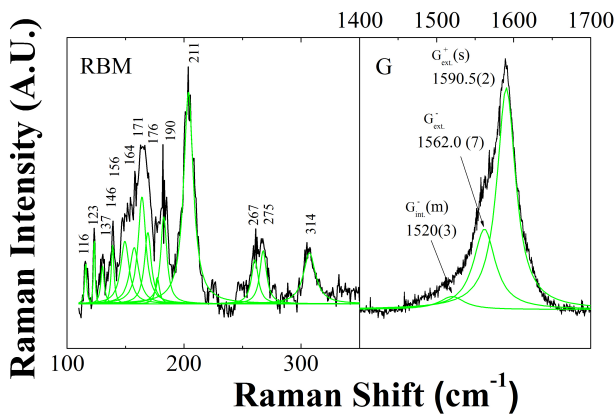
FIGURE 3. Left: Raman spectra of RBMs of DWCNTs at room temperature showing the positions of all peaks fitted with Lorentzian lineshape. Right: Raman spectra of G-bands of DWC-NTs at room temperature; $G^+_{ext}(s)$ and G^-_{ext} bands are fitting with Lorentzians and the $G^-_{int}(m)$ band is adjusted by the BWF profile. The numbers in parentheses correspond to mean value of the statistical error obtained from the fit.

In order to ensure equilibrium conditions between ruby and the sample, for each used temperature T, the measurement was started after about 25 to 30 min, and then the temperature T was measured using the ruby luminescence technique [14]. In the range of the RBMs (100 to 400 cm^{-1}), for each value of T, the Raman spectrum was obtained with an acquisition time of 360 s and 5 accumulations while that, for the range of the DWCNT (1400 to 1900 cm^{-1}) the acquisition time was 180 s and 3 accumulations.

The relation used to find the temperature of the nanotubes was [14]

$$R_1(T) = R_1(T_0) - 0.158T \text{ cm}^{-1}, \qquad (1)$$

where $R_1(T_0) = 14450$ cm^{-1}is the extrapolated value at 0 K. This linear expression is valid in the range studied. The estimated accuracy is given by the spectral resolution of our spectrometer (1 cm^{-1}). The ruby spheres were immersed in the matrix of nanotubes and the laser was focused right next to the ruby. Therefore, we do not expect significant differences between the temperature of the ruby sensor and the region on the nanotubes where the laser beam is focused. The temperature was determined by Eq. (1) before and after the measurement of the Raman spectra of DWCNTs. An average uncertainty of 10 K was estimated from the differences in temperature before and after the measurement.

3. Results and discussions

3.1. Raman scattering at room temperature

Figure 3 shows the Raman spectra of DWCNTs at room temperature. In the low frequency region we observed the radial breathing modes (RBM) and in the high frequency region we observe the tangential G bands. The RBMs modes allow us the identification and characterization of nanotubes under study. It has been previously shown that the frequency of the

radial breathing mode, ω_{RBM}, varies inversely with diameter, d, at least for small tubes (< 2 nm) [15]:

$$\omega_{RBM} = \frac{A}{d}, \qquad (2)$$

where A is a constant and d is nanotube diameter. For the determination of the diameters we have use the value $A = 228.2$ cm^{-1} nm reported by Popov and Lambin [16].

Figure 3 shows the spectral region of radial breathing modes (RBM) measured with 514.5 nm (2.41 eV) excitation for the outer and inner shells of the DWCNTs. As observed, the diameters are ranging from 0.7 nm (inner) to 2.0 nm (outer) in good agreement with those reported by E. Belandría *et al.* [17]. Table I shows the frequencies and the FWHM of the Lorentzian fitted lines attributed to the RBMs, as well as the calculated chiralities and diameters. The inner and the outer tubes of a DWCNT can be either metallic (M) or semiconducting (S), therefore there are four possible combinations, which we can label as usually: M-M, M-S, S-S and S-M, where S-M indicates an S inner and M outer tube. The interplanar separation of graphite (0.335 nm according to Ref. 33) with a tolerance of 6% was used as intertubes separation to make a tentative identification of the external and internal walls, as shown in Table I. Thus, although there are some external and internal tubes in our resonant Raman spectrum, it is not possible to determine with precision which inner tube goes with which outer tube unless experiment measurements at the individual DWCNT level as has been done in earlier work by Villalpando-Paez *et al* [18]. They find that the inner-outer tube distance (0.31-0.33 nm) was less than the interlayer spacing in graphite. Therefore, the RBMs features at 314 cm^{-1} and 164 cm^{-1}, also at 190 cm^{-1} and 123 cm^{-1} separated by 0.33 nm may possibly be inner and outer on the same DWCNT. We can also observe the existence of some SWCNTs in agreement with the results of transmission electron microscopy.

The Fig. 3 shows also a typical fit over Raman spectra of G-band in our DWCNTs sample. The G band in DWC-NTs contains contributions from both the internal and external tubes, which depend on external parameters such as pressure, temperature, and applied electrical field [19]. The G band lineshape of DWCNTs is a mixture of Lorentzian lines, the frequencies of the outer tubes ($\omega_{G+} = 1590$ cm^{-1} and $\omega_{G-} = 1562$ cm^{-1}) and a metallic shoulder ($\omega_{G-} = 1520$ cm^{-1}) with a Breit-Wigner-Fano (BWF) profile [20]. The frequency value of the outer semiconducting tube (G$^+$) at room temperature is close to the values published in Refs. 21 and 22 for DWCNTs and similar to the frequency values of G$^+$ in SWCNT [23]. The simultaneous experimental observation of the outer bands of the semiconductor nanotubes (G$^+$ and G$^-$) and the bands of internal metallic nanotubes (G$^-$) is because both the inner metallic (M) and the outer semiconductors (S) tubes are in resonance with the same excitation at 2.41 eV. Using the Kataura plot is easy to see that for a laser energy of 2.41 eV and taking into account the distribution of diameters obtained through HRTEM measurements

TABLE I. RBM on DWCNTs excited at 514.5 nm. In the first and second columns show the values for different RBM frequencies and line widths, respectively. The third and fourth column is shows the experimental diameter obtained from the Eq. (2) and the theoretical diameter to from ideal cylindrical geometry with a carbon-carbon distance of 1.44 Å. In the fifth, six and seven columns are tentatively assigned indices of chirality, conductivity type and the wall type, respectively.

$\omega_{BMR}(cm^{-1})$	FWHM (cm^{-1})	$d_{exp.}$ (nm)	$d_{theo.}$ (nm)	(n,m)	Type	Inner/Outer
116	2.0	1.97	1.97	(19,9)	S	Outer
123	1.4	1.86	1.86	(14,13)	S	Outer
137	3.4	1.67	1.67	(15,9)	M	Single-wall
146	2.8	1.56	1.56	(18,3), (16,6)	M-S	Outer
156	8.7	1.46	1.46	(13,8)	S	Outer
164	9.4	1.39	1.39	(17,1)	S	Outer
171	8.0	1.34	1.34	(13,6)	S	Inner
176	7.1	1.30	1.30	(14,4)	S	Single-wall
184	4.2	1.24	1.24	(10,8)	S	Single-wall
190	6.3	1.20	1.20	(12,5)	S	Inner
211	9.8	1.08	1.07-1.09	(13,1)-(12,3)	M-M	Single-wall
267	7.1	0.86	0.86	(9,3)	M	Inner
275	6.9	0.83	0.83	(7,5)	S	Inner
314	12.4	0.73	0.73	(8,2)	M	Inner

(see Fig. 1), there are several chiral indices that are in resonance simultaneously in the branches E_{22}^S, E_{11}^M, E_{33}^S, E_{44}^S, E_{22}^M, etc.

The Raman spectra of the RBM modes also confirm that the outer tube in our DWCNT is semiconducting and the inner tube is metallic and both are in resonance for the excitation of 2.41 eV. So, if we look at Table I, the RBM at $314\,cm^{-1}$ corresponds to a metallic inner nanotube with chiral indices (8,2) and 0.73 nm diameter and according to the Kataura plot a laser energy of 2.41 eV is in resonance for this diameter with the branch E_{11}^M. Likewise the RBM at $164\,cm^{-1}$ belongs to a semiconductor external nanotube with chiral indices (17,1) and 1.39 nm diameter and is in resonance with the branch E_{22}^S. The distance between the two layers of this DWCNT is approximately 0.33 nm, which is similar to the interlayer separation in graphite (0.335 nm). From the results of Ref. 23, which establishes the frequency dependence of ω_{G+} and ω_{G-} as a function of diameter (d_t) of the nanotubes, the expected ω_{G-} values for the inner (M) and outer (S) tubes of our DWCNTs are ω_{G-}= 1530 cm^{-1} and ω_{G-}=1560 cm^{-1} respectively. We used the average values of the inner and outer diameters (d_t) of the nanotubes (1.2 and 1.9 nm respectively) obtained by TEM [4-6]. As compared with our experimental values there is a good agreement for the outer (S) tube frequency (1562 cm^{-1}) and for the inner (M) tube frequency (1520 cm^{-1}). The G$^+$ band shows almost no dependence on the diameter or chiral angle, and their frequency value is about 1591 cm^{-1} [24]. We have made the adjustments of the Raman peak at 1520 cm^{-1} with an asymmetric line shape, described by a Breit-Wigner-Fano line shape (BWF) [24]:

$$I(\omega) = I_0 \frac{[1 + (\omega - \omega_{BWF})/q\Gamma]^2}{1 + [(\omega - \omega_{BWF})/\Gamma]^2}, \qquad (3)$$

where 1/q is a measure of the interaction of the phonon with a continuum of states, while, ω_{BWF}, I_0 and Γ are the BWF peak frequency, the intensity and the broadening factor, respectively. The BWF spectral shape occurs when a discrete energy excitation level interacts with a continuum of energy excitations, causing a resonance and anti-resonance effect and thus giving rise to a non-symmetric spectral lineshape for the discrete state. We have found at room temperature a value of 1/q = -0.08. This value is smaller than previously reported values (-0.1 to -0.15) for DWCNTs by Christofilos *et al.* [25]. Since all our spectra have a very small background we think that these differences are related to a lower proportion of metallic nanotubes present in our samples that are in resonance with the excitation energy.

3.2. Raman scattering at High-temperature

Figure 4 shows the Raman spectrum of the RBMs (between 100 and 400 cm^{-1}) and the tangential (between 1400 and 1700 cm^{-1}) G bands in DWCNTs at different temperatures obtained as was indicated in the experimental section. The Raman shift of the RBMs exhibits a linear dependence with temperature (view Fig. 5) consistent with the previous reports [11-13,23]. Taking into account that, the signal to noise ratio of Raman spectra of the RBMs was not very satisfactory, and that the spectral shape is modified slightly with increasing temperature, it was difficult to follow the behavior of the RBMs modes of vibration for the whole temperature range studied. So that it was decided to focus our attention on two
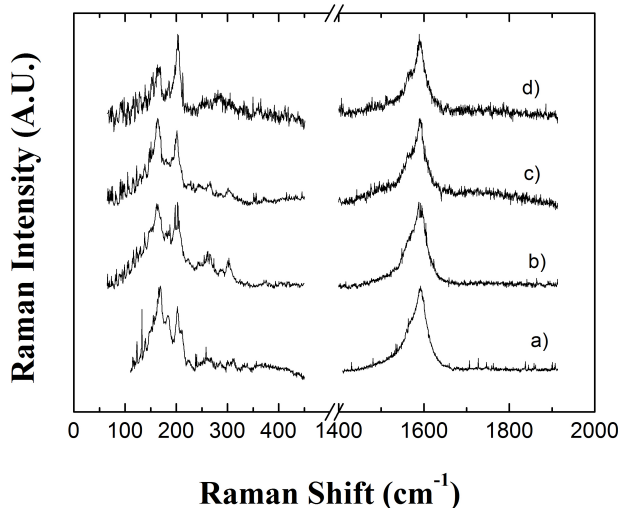
FIGURE 4. Raman spectra of RBMs and G-bands of DWCNTs at the following four temperatures: a) 319, b) 390, c) 517 y d) 653 K.
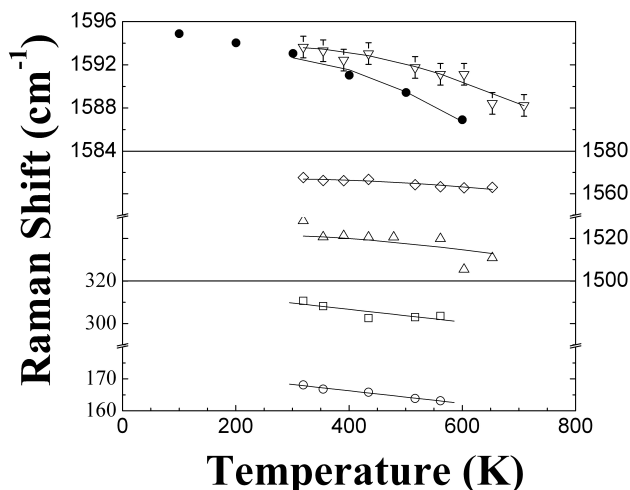
FIGURE 5. Temperature dependence of the Raman-active $G_{ext}^{+}(s)$ mode in DWCNTs. The open down triangles are our date and filled circle are from Ref. 11. Middle: temperature dependence of the Raman-active G_{ext}^{-} (diamonds) and $G_{int}^{-}(m)$ (up triangles) modes in DWCNTs. Bottom: Temperature dependence for the two Raman-active RBM modes in DWCNTs. The solid curves give the theoretical fit using the three-phonon processes and the thermal expansion contribution (Eq. (4)). The estimated errors for the Raman shift and the temperature were 1 cm^{-1} and 10 K respectively; for the sake of clarity the corresponding error bars are shown only for the $G_{ext}^{+}(s)$ mode.

representative peaks (see Fig. 5) at 171 and 314 cm^{-1}. The linear temperature coefficient values obtained for these modes are, respectively, -0.019 cm^{-1}K^{-1} and -0.029 cm^{-1}K^{-1}. These values are consistent with those reported in Ref. 26 for SWCNT bundles.

As is apparent in Fig. 4, the frequencies of the G-bands downshift with increasing temperature are in good agreement with previous work [9, 11-13]. However we note that while the qualitative behavior is similar to other works that study the temperature variation in Raman modes in SWCNTs and

DWCNTs, it is difficult to compare quantitative values because they are very sensitive to parameters such as degree of purification of nanotubes (presence of metal particles such as Co or Fe), diameter of the nanotubes, the size of the bundles and tube environment. In Fig. 5 we plot the shift of the Raman frequencies of the $G_{ext}^{+}(s)$, G_{ext}^{-} and $G_{int}^{-}(m)$ modes versus temperature for DWCNTs and a nonlinear behavior was observed clearly for the $G_{ext}^{+}(s)$ with increasing temperature. However because the scatter of experimental points is greater for the G_{ext}^{-} and $G_{int}^{-}(m)$ band modes, the nonlinearity of these tangential bands as a function of temperature is less evident. Moreover it is well known also that the nonlinearity is more important at low temperatures. Zhou et al. was the first to observe that the temperature dependence of the Raman shift for DWNTs and SWNTs have a small but clearly nonlinear dependence on temperature [11]. All previous studies showed a linear dependence with temperature for SWCNT [12-13]. However, a recent study in SWCNT shows that the $G_{ext}^{+}(s)$ peak has a universal temperature dependence (non-linear), independent of SWCNT sample type or excitation laser wavelength [26].

Returning to Fig. 5, it is seen that the values of the Raman shift obtained by Zhou et al. [11] for the $G_{ext}^{+}(s)$ mode are slightly lower than the present ones and the difference between these values increases as the temperature is increased. A reason for this behavior could be due to different thermal sensors (thermocouple and/or ruby) used to measure the temperature. We have found a statistical error for the linear coefficient of the $G_{ext}^{+}(s)$ band of about 15%. The linear coefficients shown in Table II were obtained with a second-order polynomial. It is important to note that the $G_{int}^{-}(m)$ band has a linear coefficient much larger than the other two bands $G_{ext}^{+}(s)$ and G_{ext}^{-}, this indicates that the electron-phonon interaction is more intense because of the higher carrier concentration.

The Raman shift of optical phonons with increasing temperature is due to the change of harmonic frequency with volume expansion and anharmonic coupling to phonons of other branches. The real part of the phonon self-energy shift can be written as [27]:

$$\omega(T) = \omega_0 + \Delta^{(1)}T + \Delta^{(2)}T \quad (4)$$

where $\omega_0 + \Delta^{(2)}T$ correspond to Raman shift as $T \to 0$ K, $\Delta^{(1)}T$ is the thermal-expansion contribution to the shift, and $\Delta^{(2)}T$ is due to the anharmonic coupling of the phonon in question with other phonons. The $\Delta^{(1)}T$ term can be written as [28]:

$$\Delta^{(1)}T = \omega_0 \left[\exp\left(-\gamma \int_0^T \beta(T')\,dT' \right) - 1 \right] \quad (5)$$

where γ correspond to Grüneisen parameter for the Raman mode and $\beta(T')$ is the volumetric expansion coefficient as a function of temperature T. The correction due to anharmonic

TABLE II. Parameters of fit Raman shift obtained for DWCNTs, SWCNTs, graphite and others semiconductors materials. In the third, fourth and fifth columns are representing the temperature dependent coefficients, the Grüneisen parameters and the frequency extrapolated at 0 K, respectively. Columns 6 and 7 show the coefficients of cubic (C) and quartic (D) coupling, respectively.

		$d\omega/dT$ ($\text{cm}^{-1}\text{K}^{-1}$)	γ (300 K)	ω_0 (cm^{-1})	**C** (cm^{-1})	**D** (cm^{-1})	**Ref.**
DWCNTs	G_{ext}^{+} (s)	1.3×10^{-2}	1.5	1597	-4.06	0	Our
DWCNTs	G_{ext}^{-}	-1.9×10^{-2}	1.3	1573	-6.6	0	Our
DWCNTs	G_{int}^{-} (m)	-4.3×10^{-2}	1.9	1540	-17.46	0	Our
DWCNTs	G_{ext}^{+} (s)	-2.42×10^{-3}	-1.4	1622	-26.67	0	[11]
DWCNTs	G_{ext}^{+} (s)	-2.6×10^{-2}					[9]
SWCNT	G		1.24				[36]
graphite	G	-2.4×10^{-2}	1.72-1.90	-	-	-	[9, 33, 37]
graphene	G		1.86, 1.99, 1.80				[34, 37 38]
D-CNT [†]	G_{ext}^{+}(s)	-2.3×10^{-2}					[12]
C-CNT [‡]	G_{ext}^{+}(s)	-2.8×10^{-2}					[12]
RBM		-1.9×10^{-2}	1.1	174	-1.21	0	Our
RBM		-2.9×10^{-2}	1.4	319	-3.26	0	Our
Si	LO			529	-4.24	0	[29]
Si	LO			528	-2.96	-0.174	[29]
CuGaS$_2$	Γ_5(L,T)	-5.2×10^{-3}	-0.9	75.5	-0.134	0.009	[27]
AgGaS$_2$	Γ_5(L,T)	2×10^{-3}	-4.4	35	-0.083	0.0014	[27]

[†]Discharge carbon nanotube (D-CNT).

[‡]Catalytic CNT method (C-CNT).

coupling of three-phonon processes (cubic anharmonicity in second order) can be modeled as [29-30]

$$\Delta^{(2)}T = C \left(1 + \frac{2}{e^x - 1} \right), \quad (6)$$

where $x = \hbar\omega_0/2k_BT$ correspond to coupling of two optical phonons with identical or opposite $\vec{q}$ belonging to the same branch and C is a constant.

For SWCNTs is always possible to draw a tetragonal cell, being the volume of this cell equal to

$$V = d^2 l, \quad (7)$$

where d and l are diameter and length of the nanotube, respectively. Since the coefficient of volume thermal expansion, is defined as,

$$\beta = \frac{1}{V} \left(\frac{\partial V}{\partial T} \right)_P, \quad (8)$$

then,

$$\beta = \left[\frac{1}{d^2 l} \left(\frac{\partial (d^2 l)}{\partial T} \right)_P \right]$$
$$= 2 \left[\frac{1}{d} \left(\frac{\partial d}{\partial T} \right)_P \right] + \left[\frac{1}{l} \left(\frac{\partial l}{\partial T} \right)_P \right] = 2\alpha_r + \alpha_a \quad (9)$$

where α_r and α_a are the radial and axial thermal expansion coefficients of the carbon nanotube (CNT), respectively [31].

In first approximation, we have used the values of the radial and axial thermal expansion coefficients of the CNTs for a SWCNT with a diameter of 8 Å and length of 30 Å [32]. With these values we have obtained a volumetric expansion coefficient given by:

$$\beta = -2.4608 \times 10^{-7} - 3.492 \times 10^{-8}T$$
$$+ 1.96337 \times 10^{-10}T^2 - 3.45363 \times 10^{-13}T^3$$
$$+ 3.19218 \times 10^{-16}T^4 - 1.66857 \times 10^{-19}T^5$$
$$+ 4.6717 \times 10^{-23}T^6 \quad (10)$$

With this equation (Eq. (10)), the experimental frequency shift of all the Raman modes as a function of temperature was fitted (solid line in Fig. 5) by using Eq. (4). In Fig. 6, we extrapolated the theoretical model of equation (4) at low temperatures for the G_{ext}^{-} and G_{int}^{-}(m) bands respectively. The change of the one-phonon frequency with temperature is due to the anharmonic coupling of the considered phonon with other phonons and also due to the thermal expansion of the crystal (Eq. (4)). We can clearly see that the nonlinearity is most evident for temperatures below 200 K. This occurs because the anharmonic effects tend to diminish as the temperature is reduced. Consequently, the frequency approaches to a nearly constant value as the temperature approaches zero.
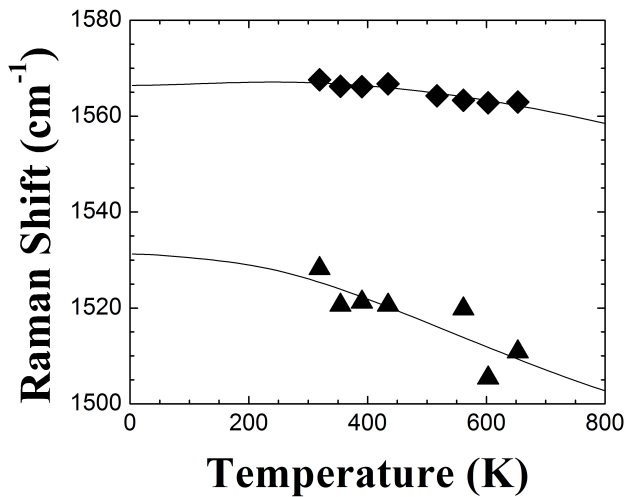
FIGURE 6. Extrapolation of the theoretical model values given by Eq. (4) at low temperatures for the G_{ext}^{-} (diamond) and $G_{int}^{-}(m)$ (up triangle) bands respectively.
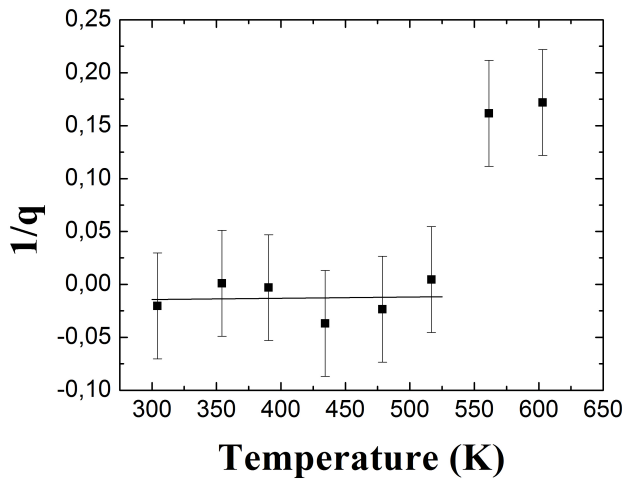
FIGURE 7. Asymmetric parameter 1/q vs. temperature for DWC-NTs. The solid curve is a linear data fitting. The error bars correspond to mean value of statistic fitting.

The adjustable parameters were γ and C. The resulting parameters are shown in Table II. As observed the absolute value of C in Eq. (6) for $G_{int}^{-}(m)$ band is the greatest of all. This indicates that the third-order anharmonic term in the lattice potential energy have an important effect in the temtemperature-dependent Raman shift for this mode. Also, we have found a Grüneisen parameter value equal to 1.5 for the $G_{ext}^{+}(s)$ band close to values reported for SWCNT, graphite and graphene (see Table II).

It is to be mentioned that the G band in SWNTs and DWCNTs both exhibits an asymmetric Breit-Wigner-Fano (BWF) line shape, which is usually an indication of an electron-phonon coupling [39,40] and not due to coupling to low-energy plasmons, as was previously reported in Ref. 35. In SWNTs, the BWF line shape is commonly used to distinguish between metallic and semiconducting tubes. Then, from the temperature dependence of the Raman peak at 1520 cm^{-1} using the BWF asymmetric line shape [24], we can calculate the variation of the parameter 1/q as a function of temperature and the resulting values are shown in Fig. 7. It is seen from this figure that the values of 1/q are nearly constant (-0.02) up to about 525 K, where a sudden jump, to a value 1/q$\approx$ 0.17, and a change of the sign in 1/q occur. A reason for this behavior would be that at 525 K there is a discontinuous increase in the Lorentzian asymmetry. This would indicate that below and/or above 525 K the electron-phonon interactions are different. However, it was found that very little information on the variation of 1/q with T for DWCNTs is available in the literature; further information on this point will be given in another work.

4. Conclusion

We have investigated the vibrational properties of DWCNTs at high temperatures. From the experimental results we observed that the frequencies of the RBMs and G-bands downshift with increasing temperature and a nonlinear behavior was observed, in good agreement with previous work. A good agreement between experimental observation and theoretical calculation confirms that the pure-temperature effect (three-phonon process) dominates the contribution to the temperature-dependent Raman shifts of RBM and G bands and the pure-volume effect is quite small within the experimental temperature range. The obtained Grüneisen parameters for the G-bands are in good agreement with the value reported for SWCNTs, graphite and graphene.

1. M.P. Anantram and F. Léonard, Rep. *Prog. Phys.* **69** (2006) 507.

2. P.J.F. Harris, *Carbon Nanotube Science synthesis, properties and applications* (Cambridge University Press, Cambridge, 2009).

3. M.S. Dresselhaus, G. Dresselhaus, and P. Avouris, *Carbon Nanotubes Synthesis, Structure, Properties and Aplications* (Springer-Verlag, Berlin, 2001).

4. E. Flahaut, A. Peigney, C. Laurent, and A. Rousset, *J. Mater. Chem.* **10** (2000) 249.

5. L. Ci *et al., Chem. Phys. Lett* **359** (2002) 63–67.

6. E. Flahaut, R. Bacsa, Alain Peigney and Christophe Laurent, *Chem. Commun.* **12** (2003) 1442.

7. J. González *et al. phys. stat. sol. (b)* **244** (2007) 136.

8. J. González *et al. Hihg Pressure Research* **28** (2008) 577.

9. S. Osswald *et al. Chem. Phys. Lett* **402** (2005) 422.

10. M.S. Dresselhaus, G. Dresselhaus, R. Saito, and A. Jorio, *Phys. Rep.* **409** (2005) 47.

11. Z. Zhou *et al. Chem. Phys. Lett.* **396** (2004) 372.

12. F. Huang *et al. J. Appl. Phys.* **84** (1998) 4022.

13. H.D. Li *et al. Appl. Phys. Lett.* **76** (2000) 2053.

14. D.D. Ragan, R. Gustavsen, and D. Schiferl, *J. Appl. Phys.* **72** (1992) 5539.

15. S. Bandow *et al.*, *Phys. Rev. Lett.* **80** (1998) 3779.

16. N. Popov and P. Lambin, *Phys. Rev. B* **73** (2006) 085407.

17. E. Belandria *et al. Carbon* **48** (2010) 2566.

18. F. Villalpando-Paez *et al. Phys. Rev. B* **82** (2010) 155416.

19. P. Puech *et al.*, *Phys. Rev. B* **72** (2005) 155436.

20. M.V. Klein, *in Light Scattering in Solids I* (Springer-Verlag, Berlin, 1983).

21. P. Puech, H. Hubel, D.J. Dunstan, R.R. Bacsa, C. Laurent, and W.S. Bacsa, *Phys. Rev. Lett.* **93** (2004) 095506.

22. J. Arvanitidis, D. Christofilos, K. Papagelis *et al., Phys. Rev. B* **71** (2005) 125404.

23. N.R. Raravikar, P. Keblinski, A.M. Rao, M.S. Dresselhaus, L.S. Schadler, and P. M. Ajayan, *Phy. Rev. B* **66** (2002) 235424.

24. A. Jorio *et al., Phys. Rev. B* **65** (2002) 155412.

25. D. Christofilos, J. Arvanitidis, and C. Tzampazis *et al. Diamond & Related Materials* **15** (2006) 1075.

26. S. Chiashi, Y. Murakami, Y. Miyauchi, and S. Maruyama, *JJAP* **47** (2008) 2010.

27. J. González *et al. Phys. Stat. Sol.* **225** (2001) R12.

28. C. Postmus, J.R. Ferraro and S.S. Mitra, *Phys. Rev.* **174** (1968) 983.

29. M. Balkanski, R.F. Wallis and E. Haro, *Phys. Rev. B* **28** (1983) 1928.

30. P.G. Klemens, *Phys. Rev.* **148** (1966) 845.

31. C. Li and T.W. Chou, *Phys. Rev. B* **71** (2005) 235414.

32. J.W. Jiang, J.S. Wang and B. Li, *Phy. Rev. B* **80** (2009) 205429.

33. M. Hanfland, H. Beister, and K. Syassen, *Phys. Rev. B* **39** (1989) 12598.

34. Y.C. Cheng, Z.Y. Zhu, G.S. Huang, and U. Schwingenschögl, *Phys. Rev. B* **83** (2011) 115449.

35. K. Kempa, *Phys. Rev. B* **66** (2002) 195406.

36. S. Reich, H. Jantoljak, and C. Thomsen, *Phys. Rev. B* **61** (2000) R13 389.

37. T.M.G. Mohiuddin *et al.*, *Phys. Rev. B* **79** (2009) 205433.

38. F. Ding *et al.*, *Nano Lett.* **10** (2010) 3453.

39. M.O. Carl, F. Hennrich, M.M. Kappes, H.V. Löhneysen, and R. Krupke, *Nano Letter* **5** (2005) 1761.

40. S. Piscanec, M. Lazzeri, F. Mauri, and A.C. Ferrari, *Eur. Phys. J. Special Topics* **148** (2007) 159.